Article

Bis(chloroacetamidino)-Derived Heteroarene-Fused Anthraquinones Bind to and Cause Proteasomal Degradation of tNOX, Leading to c-Flip Downregulation and Apoptosis in Oral Cancer Cells

Jeng Shiun Chang [1,†], Chien-Yu Chen [2,†], Alexander S. Tikhomirov [3], Atikul Islam [2], Ru-Hao Liang [2], Chia-Wei Weng [2,4], Wei-Hou Wu [2], Andrey E. Shchekotikhin [3,*] and Pin Ju Chueh [2,5,6,7,*]

[1] Department of Otolaryngology, Head and Neck Surgery, Jen-Ai Hospital, Taichung 41265, Taiwan
[2] Institute of Biomedical Sciences, National Chung Hsing University, 145 Xingda Rd., Taichung 40227, Taiwan
[3] Gause Institute of New Antibiotics, 11 B. Pirogovskaya Street, 119021 Moscow, Russia
[4] Institute of Medicine, Chung Shan Medical University, Taichung 40201, Taiwan
[5] Department of Post-Baccalaureate Medicine, College of Medicine, National Chung Hsing University, 145 Xingda Rd., Taichung 40227, Taiwan
[6] Department of Medical Research, China Medical University Hospital, Taichung 40402, Taiwan
[7] Graduate Institute of Basic Medicine, China Medical University, Taichung 40402, Taiwan
* Correspondence: shchekotikhin@mail.ru (A.E.S.); pjchueh@dragon.nchu.edu.tw (P.J.C.); Tel.: +7-499-246-0228 (A.E.S.); +886-4-22840896 (P.J.C.)
† These authors contributed equally to this work.

Simple Summary: New-generation anthraquinone derivatives attached with different heterocycles and bearing chloroacetamidines in the side chains have been synthesized to reduce side effects and drug resistance. In this study, we identified the cellular target of the studied compounds through ligand binding assays and in silico simulations. Our results illustrate that the studied compounds bound to and targeted the tumor-associated NADH oxidase (tNOX) in oral cancer cells. tNOX is a growth-related protein and is found to be expressed in cancer cells but not in non-transformed cells, and its knockdown by RNA interference in tumor cells overturns cancer phenotypes, supporting its role in cellular growth. We also identified that tNOX bound to the studied compounds and underwent degradation, which was correlated with apoptosis induction in oral cancer cells.

Abstract: Anthraquinone-based intercalating compounds, namely doxorubicin and mitoxantrone, have been used clinically based on their capacity to bind DNA and induce DNA damage. However, their applications have been limited by side effects and drug resistance. New-generation anthraquinone derivatives fused with different heterocycles have been chemically synthesized and screened for higher anticancer potency. Among the compounds reported in our previous study, 4,11-bis(2-(2-chloroacetamidine)ethylamino)anthra[2,3-b]thiophene-5,10-dione dihydrochloride (designated **2c**) was found to be apoptotic, but the direct cellular target responsible for the cytotoxicity remained unknown. Here, we report the synthesis and anticancer properties of two other derivatives, 4,11-bis(2-(2-chloroacetamidine)ethylamino)naphtho[2,3-f]indole-5,10-dione dihydrochloride (**2a**) and 4,11-bis(2-(2-chloroacetamidine)ethylamino)-2-methylanthra[2,3-b]furan-5,10-dione dihydrochloride (**2b**). We sought to identify and validate the protein target(s) of these derivatives in oral cancer cells, using molecular docking simulations and cellular thermal shift assays (CETSA). Our CETSA results illustrate that these derivatives targeted the tumor-associated NADH oxidase (tNOX, ENOX2), and their direct binding downregulated tNOX in p53-functional SAS and p53-mutated HSC-3 cells. Interestingly, the compounds targeted and downregulated tNOX to reduce SIRT1 deacetylase activity and increase Ku70 acetylation, which triggers c-Flip ubiquitination and induces apoptosis in oral cancer cells. Together, our data highlight the potential value of these heteroarene-fused anthraquinones in managing cancer by targeting tNOX and augmenting apoptosis.

1. Introduction

Anthraquinone (anthracene-9,10-dione)-based antitumor compounds have been utilized clinically for decades due to their high effectiveness against solid and hematological malignancies. The capacity of some representatives, including doxorubicin and mitoxantrone, to bind DNA and induce DNA damage/strand breaks is applied for tumor growth suppression [1–3]. However, the therapeutic action of these drugs is accompanied by side effects and the emergence of drug resistance. To address these limitations, researchers have sought to design and synthesize new generations of anthraquinone derivatives and screen them for improved anticancer properties [4,5]. Biological investigations revealed that these compounds target various molecules that are essential for tumor progression, including different secondary structures of nucleic acids, DNA topoisomerases, HDAC-6, and others [6–12]. Among the new-generation compounds, heterocyclic derivatives of anthraquinone are considered to be one of the most promising classes for the analog-based drug design of anticancer compounds [13–15]. In particular, the annellation of five-membered heterocycles with one heteroatom to 1,4-diaminoanthraquinone (an analog of mitoxantrone) yielded derivatives that retained a powerful antiproliferative profile and exhibited significantly greater activity against MDR-positive tumor cells [16]. In-depth studies showed that these compounds exerted multitarget anticancer action against tumor cells, simultaneously interacting with duplexes and G-quadruplexes of DNA, topoisomerase 1 (Top1), and Aurora B kinase to offer a potential new approach to cancer management [17–20].

Previously, we reported a set of 4,11-diaminoanthra[2,3-b]furan-5,10-diones and revealed a link between their antiproliferative potency and their ability to modulate the tNOX–NAD$^+$–SIRT1 regulatory axis [21,22]. tNOX is a growth-related tumor-associated NADH (or hydroquinone) oxidase (ENOX2) that catalyzes the generation of NAD$^+$ and is expressed in cancer cells but not in non-transformed cells [23–26]. tNOX deficiency caused by RNA interference in tumor cells can overturn cancer phenotypes, decreasing NAD$^+$ generation, proliferation, and migration/invasion while increasing apoptosis; thus, tNOX confers a growth advantage [27–32]. Given that the acetylation levels of various proteins impact many cellular functions, we further explored the functional significance of tNOX-modulated NAD$^+$ and NAD$^+$-dependent deacetylase, SIRT1, in cancer cells [21,28,32–34]. In parallel, the clinical relevance of tNOX protein expression was corroborated in serum samples from individuals with a diagnosis of malignant mesothelioma, suggesting its role as a potential malignancy detection marker [35]. By data mining in the Kaplan–Meier plotter (pan-cancer RNA-seq dataset; www.kmplot.com (accessed on 13 March 2019)), we also observed that a high tNOX expression level was correlated with a poor prognosis for overall survival in male patients with liver cancer [22]. Excitingly, numerous anticancer agents, including oxaliplatin and doxorubicin, were reported to abolish tNOX activity or downregulate tNOX expression, and this was almost invariably associated with cancer cell apoptosis and/or autophagy [21,22,29,33,34,36–39].

We observed that a substitution in the terminal group of the 4,11-side chains in generated anthraquinones seemed to play a meaningful role in tNOX/SIRT1 inhibition and apoptosis induction; in particular, the introduction of methyl or 2-hydroxy radicals in the terminal amines contributed to tNOX downregulation, whereas guanidination dramatically abrogated this property [21,22]. Taking advantage of the ability of highly basic chloroacetamidine groups to form several H-bonds and strong ionic interactions to improve binding affinity and highly lipophilic acetamidines to penetrate into tumor cells [40], we herein synthesized and evaluated the anticancer activity of anthraquinone derivatives fused with different heterocycles and bearing 2-chloroacetamidine groups in the

terminal positions of their side chains. We found that tNOX bound with these derivatives and underwent downregulation, and this was correlated with apoptosis induction in p53-functional SAS and p53-mutated HSC-3 oral cancer cells.

2. Materials and Methods

2.1. Chemistry

All solvents, chemicals, and reagents were obtained commercially and used without purification. Analytical TLC was performed on Silica Gel F_{254} plates (Merck), and column chromatography was performed using SilicaGel Merck 60. Melting points were determined using a Buchi SMP-20 apparatus and are given uncorrected. ^{1}H and ^{13}C NMR spectra were recorded on a Varian Mercury 400 Plus instrument operated at 400 MHz and 100 MHz, respectively. Chemical shifts were measured in DMSO-d_6 using tetramethylsilane as an internal standard. High-resolution mass spectra were recorded with electron spray ionization (ESI) on a Bruker Daltonics microOTOF-QII instrument. HPLC was performed using a Shimadzu Class-VP V6.12SP1 system. All solutions were evaporated under reduced pressure using an IKA RV 10 rotary evaporator at <45 °C. All products were vacuum-dried at room temperature. The purity of the final samples of 4,11-bis(2-(2-chloroacetamidine)ethylamino)naphtho[2,3-f]indole-5,10-dione dihydrochloride (designated derivative **2a**), 4,11-bis(2-(2-chloroacetamidine)ethylamino)-2-methylanthra[2,3-b]furan-5,10-dione dihydrochloride (derivative **2b**), and 4,11-bis(2-(2-chloroacetamidine)ethylamino)anthra[2,3-b]thiophene-5,10-dione dihydrochloride (derivative **2c**) was >95%, as determined by HPLC analysis.

2.2. 4,11-bis(2-(2-chloroacetamidine)ethylamino)naphtho[2,3-f]indole-5,10-dione dihydrochloride (**2a**)

A solution of 4,11-bis[(2-aminoethyl)amino]naphtho[2,3-f]indole-5,10-dione (**1a**, 100 mg, 0.26 mmol) [41], ethyl 2-chloroacetimidate hydrochloride (0.2 g, 1.3 mmol), and diisopropylethylamine (DIPEA, 0.23 mL, 1.3 mmol) in a mixture of DMSO (10.0 mL) and methanol (10.0 mL) was stirred for 3 h at 50 °C. Reaction mixture was cooled and quenched with acetone. The dark blue precipitate was filtered off and purified by column chromatography on silica gel (CHCl$_3$–MeOH–HCO$_2$H, 80:20:2 v/v). The residue was dissolved in a mixture of water (1 mL) and MeOH (3 mL), and a solution of 1 N HCl in MeOH (0.2 mL) was added. The product was precipitated with an excess of acetone, filtered off, washed with acetone (10 mL) and ether (5 mL), and dried in vacuum. The yield of compound **2a** as dihydrochloride salt was 71 mg (47%) as a dark blue powder, mp > 250 °C (decomp). HPLC Kromasil-100-5-mkm C-18 column (4.6 × 250 mm, LW = 260 nm), eluent: A—H$_3$PO$_4$ (0.01 M), B—MeCN; gradient B 15→40% (20 min), 40→70% (10 min), elution time 12.1 min, purity 98%. ^{1}H NMR (400 MHz, DMSO-d_6) δ 12.45 (s, 1H, 1-H); 10.42 (s, 1H, Ar-NH); 10.31 (s, 1H, Ar-NH); 9.82 (s, 1H, NH); 9.77 (s, 1H, NH); 9.73 (s, 1H, NH); 9.66 (s, 1H, NH); 8.28–8.24 (m, 2H, 6,9-H); 7.75–7.71 (m, 2H, 7,8-H); 7.56 (s, 1H, 3-H); 7.14 (s, 1H, 2-H); 4.42 (2H, s, CH$_2$Cl); 4.30 (2H, s, CH$_2$Cl); 4.11 (4H, br s, 2CH$_2$); 3.81–3.72 (4H, m, 2CH$_2$). ^{13}C NMR (100 MHz, DMSO-d_6) δ 179.4 (C=O), 177.8 (C=O), 162.5 (C), 162.3 (C), 147.8 (C), 141.9 (C), 134.8 (C), 134.3 (C), 131.8 (CH), 131.4 (CH), 128.2 (CH), 128.1 (CH), 125.7 (2CH), 107.6 (C), 106.5 (C), 103.4 (C), 46.5 (CH$_2$), 45.4 (CH$_2$), 43.6 (CH$_2$), 43.2 (CH$_2$), 42.3 (CH$_2$), 42.2 (CH$_2$). HRMS (ESI) calculated for C$_{24}$H$_{25}$Cl$_2$N$_6$O$_2$S C$_{24}$H$_{26}$Cl$_2$N$_7$O$_2$ [M + H]$^+$ 514.1520, found 514.1535.

2.3. 4,11-bis(2-(2-chloroacetamidine)ethylamino)-2-methylanthra[2,3-b]furan-5,10-dione dihydrochloride (**2b**)

This compound was prepared from **1b** [21] as described for **2b**. The yield of compound **2b** as dihydrochloride salt was 78 mg (50%) as a dark blue powder, mp > 250 °C (decomp). HPLC Kromasil-100-5-mkm C-18 column (4.6 × 250 mm, LW = 260 nm), eluent: A—H$_3$PO$_4$ (0.01 M), B—MeCN; gradient B 15→40% (20 min), 40→70% (10 min), elution time 13.3 min, purity 95%. ^{1}H NMR (400 MHz, CD$_3$OD) δ 8.18–8.15 (m, 2H, 6,9-H); 7.69–7.67 (m, 2H, 7,8-H); 6.85 (s, 1H, 3-H); 4.49 (s, 2H, CH$_2$Cl); 4.41 (s, 2H, CH$_2$Cl); 4.14–4.11 (2H, m, CH$_2$); 3.99–3.97 (2H, m, CH$_2$); 3.79–3.77 (2H, m, CH$_2$); 3.73–3.71 (2H, m, CH$_2$); 2.47 (3H, s, CH$_3$).

^{1}H NMR (400 MHz, DMSO-d_6) δ 12.31 (br s, 1H, Ar-NH); 11.79 (br s, 1H, Ar-NH); 10.54 (s, 1H, NH); 10.43 (s, 1H, NH); 9.72–9.71 (m, 2H, NH$_2$); 9.44 (s, 1H, NH$_2$); 9.36 (s, 1H, NH$_2$); 8.25–8.22 (m, 2H, 6,9-H); 7.76–7.74 (m, 2H, 7,8-H); 7.22 (s, 1H, 3-H); 4.50 (2H, s, CH$_2$Cl); 4.48 (2H, s, CH$_2$Cl); 4.09 (2H, br s, CH$_2$); 3.98–3.94 (2H, m, CH$_2$); 3.59–3.56 (H, m, CH$_2$); 3.55–3.51 (H, m, CH$_2$); 2.49 (3H, s, CH$_3$). ^{13}C NMR (100 MHz, DMSO-d_6) δ 180.9 (C=O), 179.3 (C=O), 162.4 (C), 162.2 (C), 150.0 (C), 148.5 (C); 144.7 (CH); 136.7 (C), 134.1 (C), 133.8 (C); 132.7 (CH), 132.4 (CH), 125.9 (CH), 125.8 (CH), 121.1 (C); 111.9 (C); 108.4 (C); 105.6 (C); 46.9 (CH$_2$), 45.8 (CH$_2$), 44.4 (CH$_2$), 44.1 (CH$_2$), 41.9 (CH$_2$), 41.0 (CH$_2$); 13.6 (CH$_3$). HRMS (ESI) calculated for C$_{25}$H$_{27}$Cl$_2$N$_6$O$_3$ [M + H]$^+$ 529.1516, found 529.1542.

2.4. 4,11-bis(2-(2-chloroacetamidine)ethylamino)anthra[2,3-b]thiophene-5,10-dione dihydrochloride (2c)

This compound was prepared from **1c** [42] as described for **2c**. The yield of compound **2c** as dihydrochloride salt was 78 mg (45%) as a dark blue powder, mp > 250 °C (decomp). HPLC Kromasil-100-5-mkm C-18 column (4.6 × 250 mm, LW = 260 nm), eluent: A—H$_3$PO$_4$ (0.01 M), B—MeCN; gradient B 10→50% (30 min), elution time 15.9 min, purity 95%.^{1}H NMR (400 MHz, DMSO-d_6) δ 11.93 (br s, 2H, 2Ar-NH); 10.73–10.70 (m, 2H, 2NH); 10.00–9.98 (m, 2H, NH$_2$); 9.67–9.65 (m, 2H, NH$_2$); 8.19–8.16 (m, 3H, 2,6,9-H); 7.95 (d, 1H, J = 4.4, 3-H); 7.74–7.72 (m, 2H, 7,8-H); 4.54 (2H, s, CH$_2$Cl); 4.53 (2H, s, CH$_2$Cl); 4.10–4.09 (2H, m, CH$_2$); 3.95–3.94 (2H, m, CH$_2$); 3.73–3.70 (4H, m, 2CH$_2$). ^{13}C NMR (100 MHz, DMSO-d_6) δ 180.7 (2C=O), 163.0 (C), 162.9 (C), 146.0 (C), 145.1 (C), 135.5 (C), 135.2 (C), 134.0 (C), 133.9 (C), 108.2 (C), 106.8 (C), 132.4 (2CH), 131.4 (CH), 126.0 (CH), 125.8 (2CH), 45.0 (CH$_2$), 43.2 (CH$_2$), 43.1 (CH$_2$), 43.0 (CH$_2$), 38.9 (2CH$_2$). HRMS (ESI) calculated for C$_{24}$H$_{25}$Cl$_2$N$_6$O$_2$S [M + H]$^+$ 531.1131, found 531.1140.

2.5. Cell Culture and Reagents

The anti-PARP, anti-Bcl2, anti-c-Flip, anti-ADP-ribose, anti-γH2AX, and anti-caspase 8 antibodies were purchased from Cell Signaling Technology, Inc. (Beverly, MA, USA). The anti-β-actin antibody was from Millipore Corp. (Temecula, CA, USA). The anti-ubiquitin antibody was purchased from Santa Cruz Biotechnology, Inc. (Santa Cruz, CA, USA). The anti-Ku70 and anti-acetyl-Ku70 antibodies were from Arigo Biolaboratories (Hsinchu, Taiwan). The commercially available anti-ENOX2 (a.k.a. tNOX, COVA1) antibody from Proteintech (Rosemont, IL, USA) was used for immunoprecipitation. The antisera to tNOX used for immunoblotting were generated as described previously [43]. The anti-mouse and anti-rabbit IgG antibodies and other chemicals were purchased from Sigma Chemical Company (St. Louis, MO, USA) unless otherwise specified.

SAS (human squamous cell carcinoma of the tongue) and HSC-3 (human tongue squamous cell carcinoma) cells were grown in Dulbecco's Modified Eagle Medium (DMEM), and were kindly provided by Dr. Yuen-Chun Li (Department of Biomedical Sciences, Chung Shan Medical University, Taiwan). Media were supplemented with 10% FBS, 100 units/mL penicillin, and 50 μg/mL streptomycin. Cells were maintained at 37 °C in a humidified atmosphere of 5% CO$_2$ in air, and the media were replaced every 2–3 days. Cells were treated with different concentrations of individual derivatives (dissolved in water), as described in the text, or with the same volume of water (vehicle control).

2.6. Continuous Monitoring of Cell Growth by Cell Impedance Measurements

For continuous monitoring of changes in cell growth, cells (7.5 × 10^3 cells/well) were seeded onto E-plates and incubated for 30 min at room temperature, and then the E-plates were placed onto the xCELLigence System (Roche, Mannheim, Germany). Cells were grown overnight and then exposed to different derivatives or water, and impedance was measured every hour, as previously described [32]. Cell impedance was defined by the cell index (CI) = (Z$_i$ − Z$_0$) [Ohm]/15[Ohm], where Z$_0$ is background resistance and Z$_i$ is the resistance at an individual time point. A normalized cell index was determined

as the cell index at a certain time point (CI_{ti}) divided by that at the normalization time point (CI_{nml_time}).

2.7. Apoptosis Determination

Apoptosis was measured using an Annexin V-FITC Apoptosis Detection Kit (BD Pharmingen, San Jose, CA, USA). Cells cultured in 6 cm dishes were trypsinized and collected by centrifugation. The cell pellet was washed, resuspended in $1\times$ binding buffer, and stained with annexin V-FITC (fluorescein isothiocyanate), as recommended by the manufacturer. Cells were also stained with propidium iodide (PI) to detect necrosis or late apoptosis. Early apoptotic cells are Annexin V-FITC-positive and PI-negative, whereas late apoptotic cells are Annexin V-FITC and PI double-positive, analyzed using a Beckman Coulter FC500 flow cytometer.

2.8. Reverse Transcriptase–Polymerase Chain Reaction (RT-PCR)

Total RNA from oral cancer cells was isolated using the TRIzol reagent (Gibco, Carlsbad, CA, USA). First-strand cDNA was synthesized from 1 μg of total RNA using Superscript II (Life Technologies, Rockville, MD, USA). The primers for tNOX (NCBI Reference Sequence: XM_034949457.1) were used for PCR amplifications: 5′-GCTGTGCTTCTAGGCTGTGT-3′ (sense) and 5′-TTATCAAGACGGTGCAAGTAGGA-3′ (antisense), while GADPH (NCBI Reference Sequence: NM_001411843.1) were 5′-GGAAGGCCATGCCAGTGAGC-3′ (sense) and 5′-TATCGTGGAAGGACTCATGA-3′ (antisense). The reaction conditions consisted of 30 cycles of 95 °C for 30 s, 55 °C for 30 s, and 72 °C for 1 min, followed by a final extension of 5 min at 72 °C. The obtained PCR products were resolved by 1.4% agarose gel electrophoresis and visualized by DNA View nucleic acid staining.

2.9. Identification of tNOX as a Cellular Target by Cellular Thermal Shift Assays (CETSA)

The ability of each derivative to target intracellular tNOX was established by CETSA. Briefly, cells (2×10^7) were seeded in 10 cm cultured dishes, cultured for 24 h, pretreated with 10 μM MG132 for 1 h, washed with PBS, treated with trypsin, and collected. The samples were centrifuged at $12,000\times g$ rpm for 3 min at room temperature, the pellets were gently resuspended with 1 mL of PBS, and the samples were centrifuged at $7500\times g$ rpm for 3 min at room temperature. The pellets were resuspended with 1 mL of PBS containing 20 mM Tris-HCl, pH 7.4, 100 mM NaCl, 5 mM EDTA, 2 mM phenylmethylsulfonyl fluoride (PMSF), 10 ng/mL leupeptin, and 10 μg/mL aprotinin. The samples were transferred to Eppendorf tubes and subjected to three freeze–thaw cycles; for each cycle, the tubes were exposed to liquid nitrogen for 3 min, placed in a heating block at 37 °C for 3 min, and vortexed briefly. For the experimental sample set, each individual derivative was added to a final concentration of 20 μM; for the control sample set, the same volume of vesicle solvent was added. The samples were heated at 37 °C for 1 h and dispensed to 100 μL aliquots. Pairs consisting of one control aliquot and one experimental aliquot were heated at 40 °C, 43 °C, 46 °C, 49 °C, 52 °C, 55 °C, 58 °C, 61 °C, or 67 °C for 3 min. Insoluble proteins were separated by centrifugation at $12,000\times g$ rpm for 30 min at 4 °C, and the soluble protein-containing supernatants were resolved by SDS-PAGE and subjected to Western blot analysis using antisera to tNOX [27,43]. β-actin was detected as a loading control.

2.10. Immunoblotting and Immunoprecipitation

Cell extracts were prepared in lysis buffer (20 mM Tris-HCl pH 7.4, 100 mM NaCl, 5 mM EDTA, 2 mM phenylmethylsulfonyl fluoride (PMSF), 10 ng/mL leupeptin, 10 μg/mL aprotinin). Volumes of extract containing equal amounts of proteins (40 μg) were applied to SDS-PAGE gels, and resolved proteins were transferred to PVDF membranes (Schleicher & Schuell, Keene, NH, USA). The membranes were blocked, washed, and probed with a primary antibody. After washing to remove unbound primary antibody, membranes were incubated with horseradish peroxidase-conjugated secondary antibody for 1 h. The blots

were washed again and developed using enhanced chemiluminescence (ECL) reagents, according to the manufacturer's protocol (Amersham Biosciences, Piscataway, NJ, USA).

For immunoprecipitation, protein extracts from 100 mm dishes were incubated with 20 μL of Protein G Agarose Beads (for rabbit antibodies) for 1 h at 4 °C in rotation for pre-clearing. Then, 30 μg of supernatants was collected to use as input (control). Ubiquitin antibodies or control IgG were added into the supernatants and incubated onto beads in 500 μL of PBS-Tween 20 1% for overnight in rotation at 4 °C. Beads were precipitated by centrifugation at $3000\times g$ rpm, 2 min at 4 °C. Beads were washed twice with lysis buffer and samples were prepared for Western blotting analysis.

2.11. Molecular Docking Simulation

The chemical structures of the derivatives were constructed using the MolView server and saved in SDF format [44]. The predicted full-length structure of human tNOX was downloaded from the AlphaFold Protein Structure Database and used for this docking study [45]. Molecular docking was performed with parameters of population size = 1500, generations = 80, and numbers of solutions = 3, and the docking energy was calculated using the iGEMDOCK software [46]. The docking poses of derivatives were analyzed using PyMol version 2.0.4 (https://pymol.org/2/ (accessed on 18 May 2022); PyMOL Molecular Graphics System, Schrodinger, New York, NY). The interaction diagram was generated using the BIOVIA Discovery Studio Visualizer (https://discover.3ds.com/discovery-studio-visualizer-download (accessed on 18 May 2022); Dassault System, San Diego, CA, USA).

2.12. Statistics

All data are expressed as the means $\pm$ SEs of three independent experiments. The significance of differences between control and treatment groups was calculated using a one-way ANOVA.

3. Results

3.1. Synthesis of Heteroarene-Fused Anthraquinones

Starting anthraquinone derivatives **1a–c**, which were annealed with pyrrole, furan, and thiophene, respectively, were synthesized in accordance with our previously reported multistep procedures [21,41,42]. The terminal amino groups of the 4,11-side chains can be converted to acetamidines by reaction with an appropriate iminoester [40,47]. Here, mild heating of amines **1a–c** with 2-chloroacetimidate hydrochloride in the presence of Hünig's base (diisopropylethylamine, DIPEA) was used to generate 4,11-bis(2-(2-chloroacetamidine)ethyl)amine derivatives of heteroarene-fused anthraquinones (**2a–c**) at reasonable yields (Scheme 1) (Figure 1). Column chromatography followed by treatment with 1N HCl in methanol was used to obtain water-soluble hydrochloride salts of **2a–c**. The assigned structures of **2a–c** were confirmed by ^{1}H and ^{13}C NMR; the purity of the final samples was >95% (Figure S1 in Supplementary Materials).

3.2. Bis(chloroacetamidino)heteroarene-Fused Anthraquinones Attenuate the Proliferation of Oral Cancer Cells through Induction of Apoptosis

To explore whether heteroarene-fused anthraquinones **2a–c** possess anticancer properties against oral cancer cells, we used cell impedance measurement to evaluate the cell growth profiles of two human oral squamous carcinoma cell lines with varied p53 functionality: SAS and HSC-3 cells. We chose these lines to additionally determine whether p53 functionality affects the anticancer property of these derivatives. In SAS cells, p53 is expressed as a truncated version due to an early stop codon, but its ability to be phosphorylated at serine 46 sustains its apoptotic activity (http://p53.free.fr/Database/Cancer_cell_lines/p53_cell_lines.html (accessed on 18 May 2022)). In HSC-3 cells, in contrast, a defect in the serine 46 phosphorylation of p53 in HSC-3 cells contributes to a faulty transcriptional activation of proapoptotic genes [48,49]. Our results validate that the three derivatives attenuated the growth of SAS cells, showing comparable levels of inhibition at 0.5 and

2 μM, and that the growth inhibition was similar across all three derivatives (Figure 2A–C). Contrastingly, the derivatives exhibited less cytotoxicity against p53-mutated HSC-3 cells compared to SAS cells, and **2b** displayed markedly weaker inhibition than the other two derivatives at 0.5 μM (Figure 2D–F).

2a X = NH, R = H (47%);
2b X = O, R = CH$_3$ (50%);
2c X = S, R = H (45%).
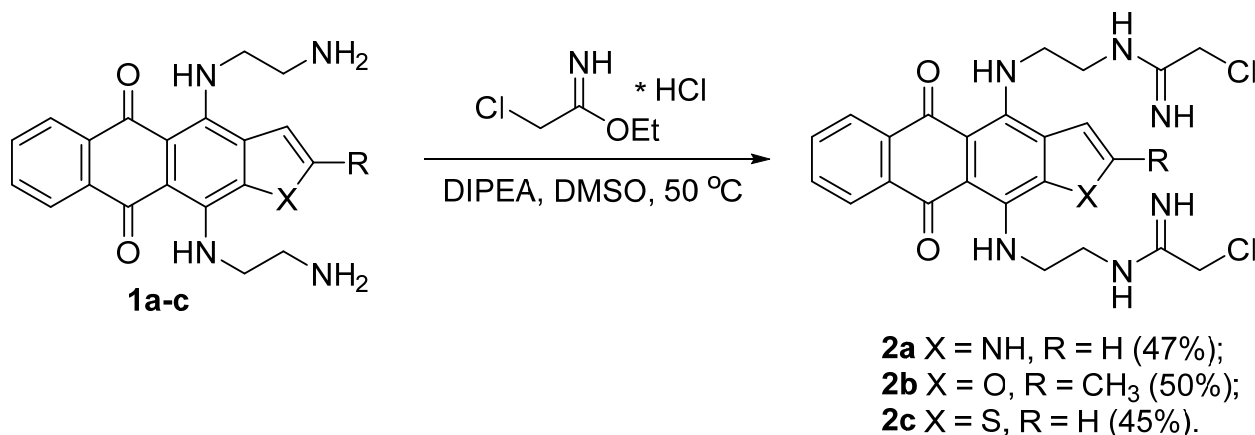
Scheme 1. Synthesis of 4,11-bis(2-(2-chloroacetamidine)ethyl)amine derivatives of heteroarene-fused anthraquinones, designated as **2a–c**.
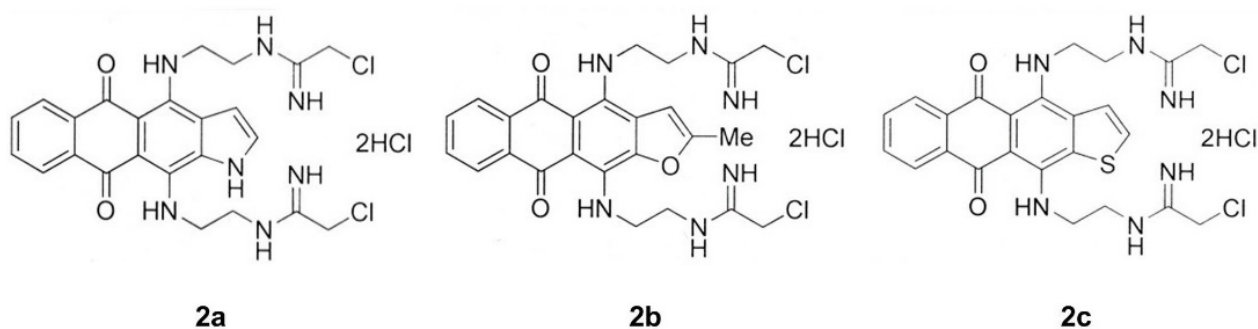

Figure 1. Structures of bis(chloroacetamidino)heteroareneanthraquinones **2a–c**.

Next, the mechanisms underlying the cytotoxicity of these derivatives were explored, particularly in the p53-independent scenario. This is the first report on the anticancer properties of **2a** or **2b**, while **2c** was previously shown to exert apoptotic activity on bladder cancer cells [40]. Here, we report that all three compounds provoked noticeable increases in the apoptotic populations of both cell lines at 0.5 or 2 μM, as assessed by Annexin V and PI staining (Figure 3A). The apoptotic activity of these derivatives was supported by Western blot analysis, which showed enhancement of caspase 3-directed PARP cleavage, the ADP-ribosylation of PARP, and γH$_2$AX (a DNA damage marker) (Figure 3B). The uncropped blots and molecular weight markers are shown in Supplementary Figure S2. The cytotoxic effect of these derivatives was also evidenced by the downregulation of anti-apoptotic Bcl-2 and c-Flip and a concurrent induction of cleaved caspase 8 in SAS p53-functional cells (Figure 3B). Interestingly, c-Flip downregulation was also observed in HSC-3 p53-mutated cells, suggesting that the studied derivatives could trigger a p53-dependent and/or p53-independent apoptotic mechanism (Figure 3B). The degradation of c-Flip is regulated by SIRT1-mediated Ku70 deacetylation, which leads to cell death [50,51]. Consistent with this, we found that the heteroarene-fused anthraquinone **2c** enhanced the acetylated Ku70 levels in both cell lines (Figure 3C). However, SIRT1 expression seemed to be unchanged in cells treated with the derivatives (Figure 3B). The lack of alteration in SIRT1 expression suggested that there may be a different (non-SIRT1) upstream regulator.
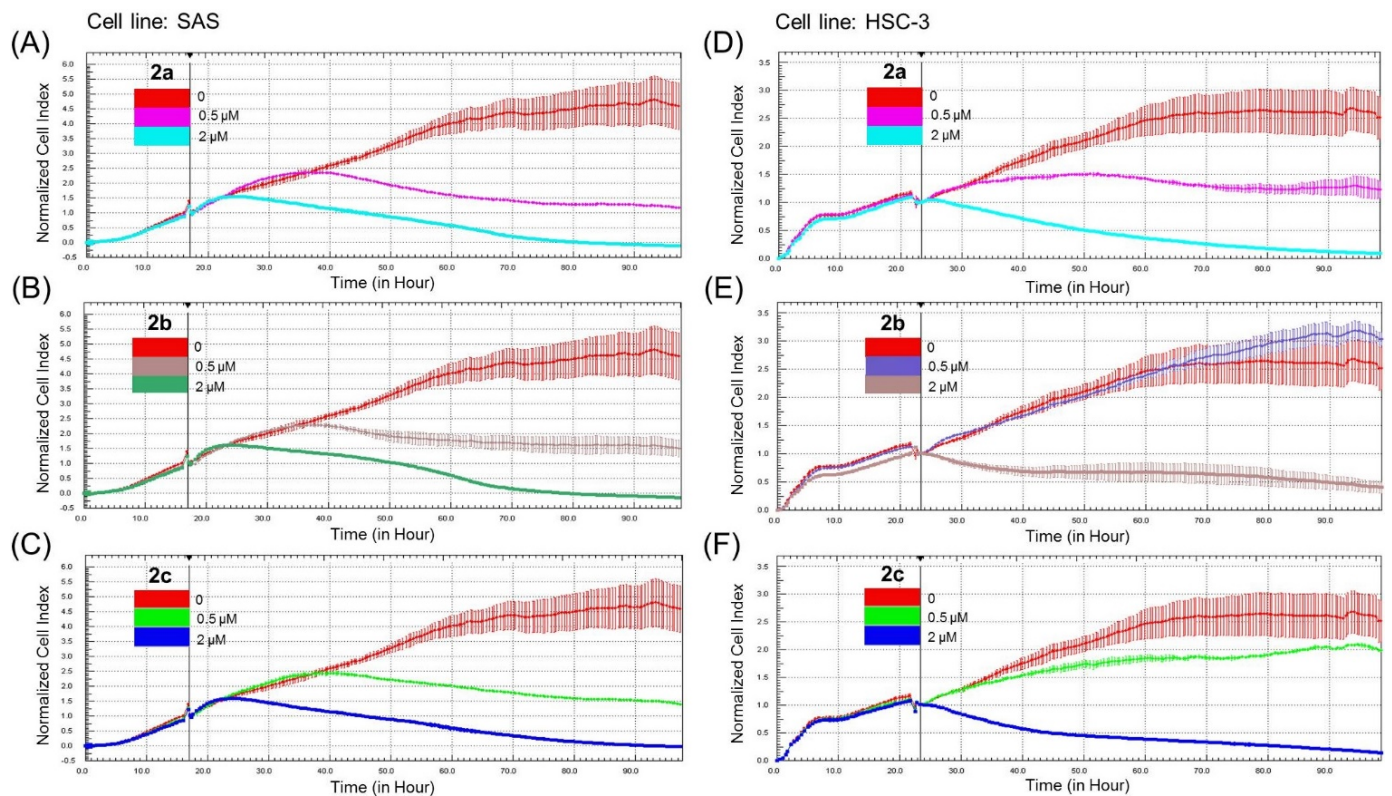
Figure 2. Bis(chloroacetamidino)heteroareneanthraquinones **2a–c** attenuate the growth of oral cancer cells. Cell proliferation was dynamically monitored by impedance measurements in SAS (**A**–**C**) and HSC-3 (**D**–**F**) cells, as described in the Materials and Methods. Shown are normalized cell index values measured. Cells were treated with various concentrations of the studied derivatives **2a–c**.

3.3. Bis(chloroacetamidino)heteroarene-Fused Anthraquinones Downregulate tNOX Expression at the Transcriptional and Protein Levels

To address whether the derivatives use a different upstream regulator to alter c-Flip, we explored the role of tNOX in our system, given that the tNOX–NAD⁺–SIRT1 regulatory axis contributes to the antiproliferative potency and apoptosis induction of 4,11-diaminoanthra[2,3-b]furan-5,10-diones [21,22]. Indeed, we found that tNOX expression was suppressed by the heteroarene-fused anthraquinones at the protein level in both cell lines (Figure 4A). The uncropped blots and molecular weight markers are shown in Supplementary Figure S3. Moreover, pre-treatment with the proteasome inhibitor, MG132, considerably rescued the stability of tNOX, suggesting that the proteasome contributes to the tNOX degradation triggered by **2c** in both cell lines (Figure 4B). We next confirmed that tNOX was ubiquitinated in SAS cells by performing immunoprecipitation experiments with a commercially available antibody against endogenous tNOX and immunoblotting with an anti-ubiquitin antibody. It was evident that the total tNOX protein was reduced while its ubiquitin level was augmented in **2c**-exposed cells compared to controls (Figure 4C). However, the lysosome inhibitor, chloroquine, failed to reverse the 2c-triggered tNOX downregulation in HSC-3 cells, indicating that the autophagy–lysosome system might not be important for this process (Figure 4D). Derivative **2c** at 1 and 2 μM was also found to significantly reduce the transcriptional level of tNOX in SAS and HSC-3 cells (Figure 4E). These lines of evidence indicated that the heteroarene-fused anthraquinones induced tNOX transcriptional downregulation and proteasomal, but not lysosomal, degradation.
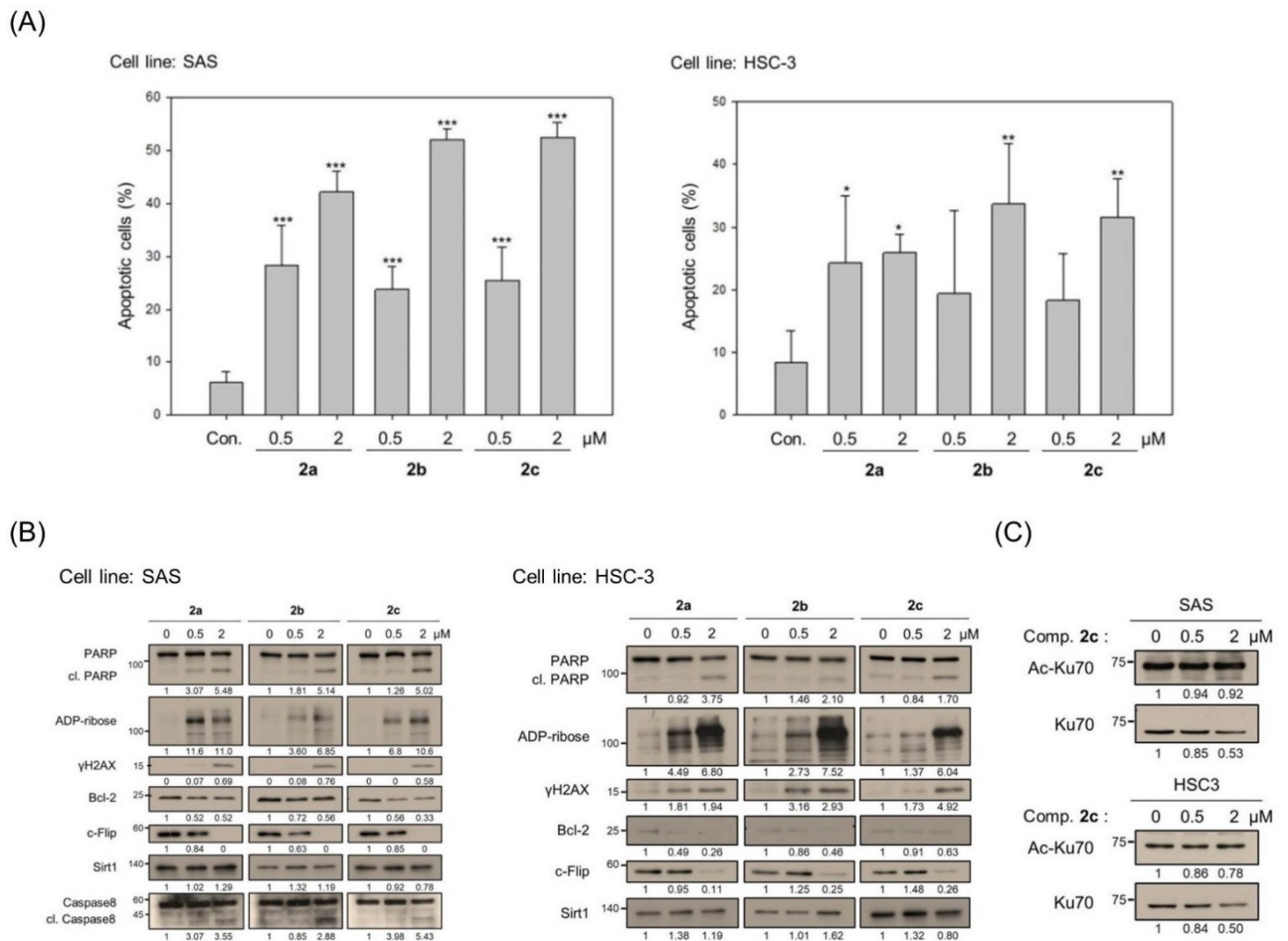
Figure 3. Bis(chloroacetamidino)heteroareneanthraquinones **2a–c** provoke apoptosis in oral cancer cells. Cells were exposed to compounds at various concentrations for 24 h. (**A**) The percentage of apoptotic cells was determined by flow cytometry with Annexin V-FITC and PJ staining, and the results are presented as the percentage of apoptotic cells. Values (means ± SDs) are from at least three independent experiments (* $p < 0.05$, ** $p < 0.01$, *** $p < 0.001$). (**B**) Cells were treated with bis(chloroacetamidino)heteroareneanthraquinones **2a–c** for various concentrations, and aliquots of cell lysates were resolved by SDS-PAGE and analyzed for protein expression by Western blotting. β-actin was used as an internal loading control to monitor for equal loading. Representative images are provided from at least three independent experiments. (**C**) Cells were treated with the derivative **2c** for various concentrations, and aliquots of cell lysates were resolved by SDS-PAGE and analyzed for protein expression by Western blotting. β-actin was used as an internal loading control to monitor for equal loading. Representative images are provided from at least three independent experiments. The uncropped blots and molecular weight markers are shown in Supplementary Figure S2.
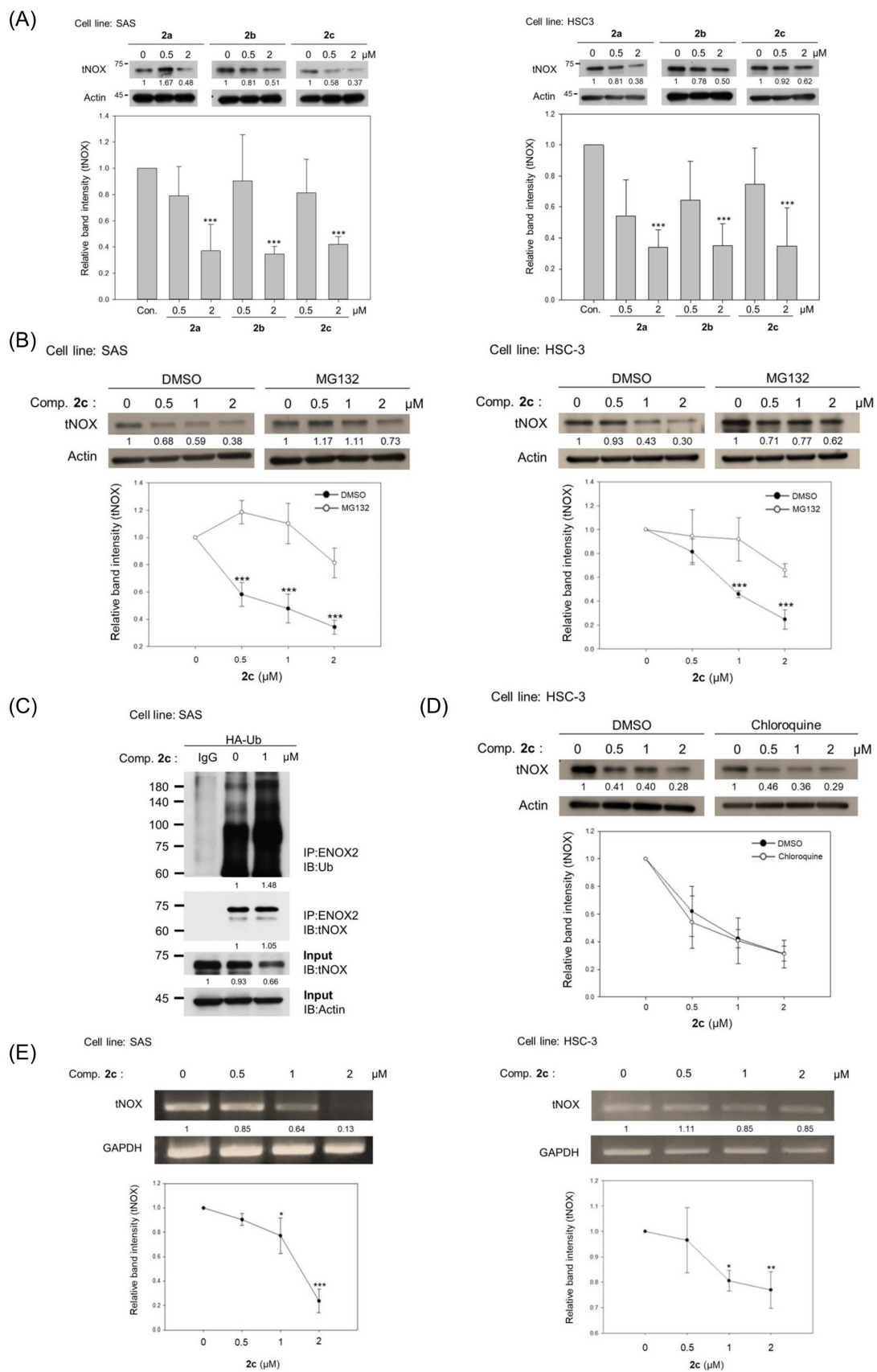
Figure 4. Bis(chloroacetamidino)heteroareneanthraquinones **2a–c** downregulate tNOX expression. (**A**) Bis(chloroacetamidino)heteroareneanthraquinones **2a–c** markedly inhibited tNOX protein expression

analyzed by Western blotting in SAS and HSC-3 cells. (**B**) Bis(chloroacetamidino)heteroareneanthraquinones **2c**-inhibited tNOX expression was reversed by the proteasome inhibitor, MG132, in SAS and HSC-3 cells. Aliquots of cell lysates were resolved by SDS-PAGE and analyzed by Western blotting. β-actin was detected as an internal control. Representative images are shown. Values (means ± SDs) are from at least three independent experiments (** $p < 0.01$, *** $p < 0.001$). (**C**) The lysates of HA-Ub overexpressing SAS cells were immunoprecipitated with nonimmune IgG or an antibody against ENOX2 (tNOX), and the bound proteins were detected by Western blotting with anti-ubiquitin or anti-tNOX antibodies. The total lysates were also immunoblotting with anti-tNOX or anti-β-actin antibodies. Aliquots of cell lysates were resolved by SDS-PAGE and analyzed by Western blotting. β-actin was detected as an internal control. Representative images are shown. (**D**) Bis(chloroacetamidino)heteroareneanthraquinones **2c**-inhibited tNOX expression was not reversed by the lysosome inhibitor, chloroquine (CQ), in HSC-3 cells. Aliquots of cell lysates were resolved by SDS-PAGE and analyzed by Western blotting. β-actin was detected as an internal control. Representative images are shown. (**E**) The transcript level of tNOX was reduced by the derivative **2c** analyzed by RT-PCR in SAS and HSC-3 cells. Values (means ± SDs) are from at least three independent experiments (* $p < 0.05$, ** $p < 0.01$, *** $p < 0.001$). The uncropped blots and molecular weight markers are shown in Supplementary Figure S3.

3.4. tNOX Acts as a Cellular Target of bis(chloroacetamidino)heteroarene-Fused Anthraquinones, as Shown by Cellular Thermal Shift Assays (CETSA) and Molecular Docking Simulations

To assess whether tNOX directly and physically binds to the studied derivatives in oral cancer cells, we conducted CETSA. This strategy is based on the concept that a ligand–protein interaction increases the thermal stability of the protein in its native configuration [52,53]. Without direct binding to its ligand, the protein is unfolded; thus, it is promptly precipitated upon heating and exhibits a lower melting temperature (T_m). To calculate T_m values, we first generated CETSA curves in which the intensity of tNOX protein on Western blot was plotted against the temperature. We found that **2c** treatment increased T_m from 48.1 °C to 58.2 °C in SAS cells and from 50.3 °C to 56.2 °C in HSC-3 cells; this increase of more than 5 °C in T_m indicates that **2c** prompted the thermal stabilization of tNOX through direct binding (Figure 5A). Similarly, T_m values were increased by exposure to derivative **2a** in both cell lines, reinforcing the idea that these derivatives have tNOX-binding capacity comparable to that of **2c** (Figure 5B). The derivative **2b** was also found to target tNOX in HSC-3 cells, as evidenced by T_m increasing by the exposure to derivative **2b** (Figure 5C).

To explore the binding mode between the derivatives and the predicted tNOX structure, blind docking was performed to predict the binding sites and conduct docking calculations, which were superimposed with the different orientations (Figure 6A). Our results illustrated that the three studied derivatives might bind to the same pocket of tNOX, and enabled us to predict docking energies for **2c** (−128.1 kJ/mol), **2a** (−124.9 kJ/mol), and **2b** (−118.7 kJ/mol) (Figure 6B). Among the three compounds, **2b** seemed to have the least affinity for tNOX. The heterocyclic cores of compounds **2a–c** interacted via Lys 98, Pro117, Pro118, and Tyr 180 by participating in electrostatic, hydrophobic, or van der Waals interactions, while other residues were oriented in a unique manner to each derivative. We also found that the tNOX inhibitor, LY181984, exhibited a binding mode similar to those of the derivatives, although with a much lower affinity (−100.7 kJ/mol) [54] (Figure 6B). Further analysis of the binding mode revealed that the interaction residues to LY181984 were more similar to those of **2a** than those of the other two derivatives (Figure 6C). The heteroarene-fused anthraquinones were predicted to generate more hydrogen bonds than LY181984; since hydrogen bonds could help stabilize surrounding residues, this finding could explain the weaker affinity predicted for LY181984 (Figure 6).
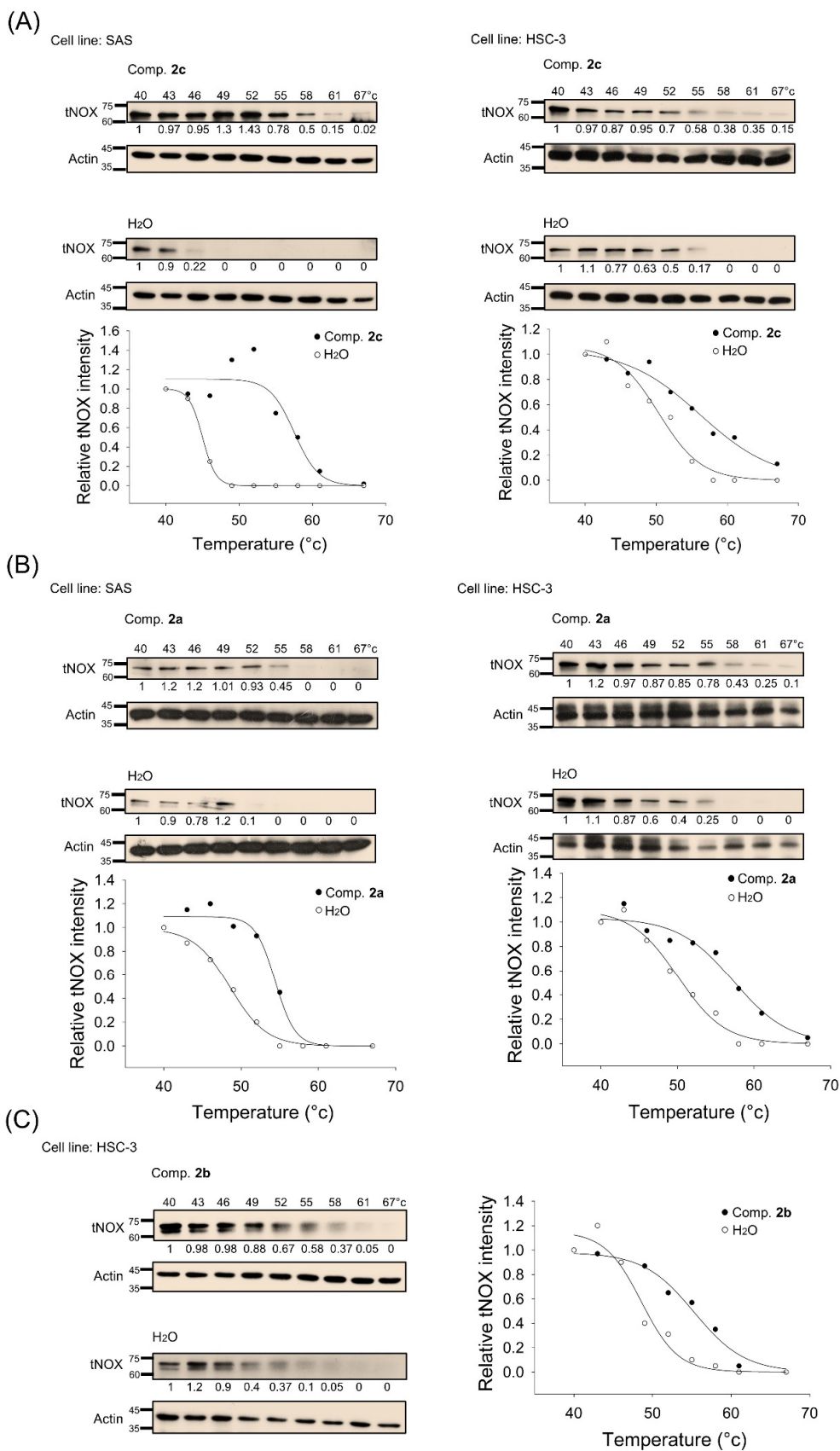
Figure 5. CETSA-based identification of direct binding between tNOX protein and bis(chloroace-tamidino)heteroarene-fused anthraquinones **2a–c**. Top panel: the immunoblot intensity of tNOX in

SAS (left panel) and HSC-3 (right panel) cells in the presence and absence of the studied derivatives **2c** (**A**) and derivative **2a** (**B**) in the CETSA experiments as described in the Materials and Methods. Aliquots of cell lysates were resolved by SDS-PAGE and analyzed for protein expression by Western blotting. β-actin was used as an internal loading control to monitor for equal loading. Representative images are shown. Bottom panel: CETSA melting curves of tNOX in the presence and absence of derivatives **2c** (**A**) and derivative **2a** (**B**) in SAS (left panel) and HSC-3 (right panel) cells. The immunoblot intensity was normalized to the intensity of the 40 °C samples. (**C**) Left panel: the immunoblot intensity of tNOX in HSC-3 cells in the presence and absence of the studied derivatives **2b** in the CETSA experiments. Right panel: CETSA melting curves of tNOX in the presence and absence of derivatives **2b** in HSC-3 cells. The uncropped blots and molecular weight markers are shown in Supplementary Figure S4.
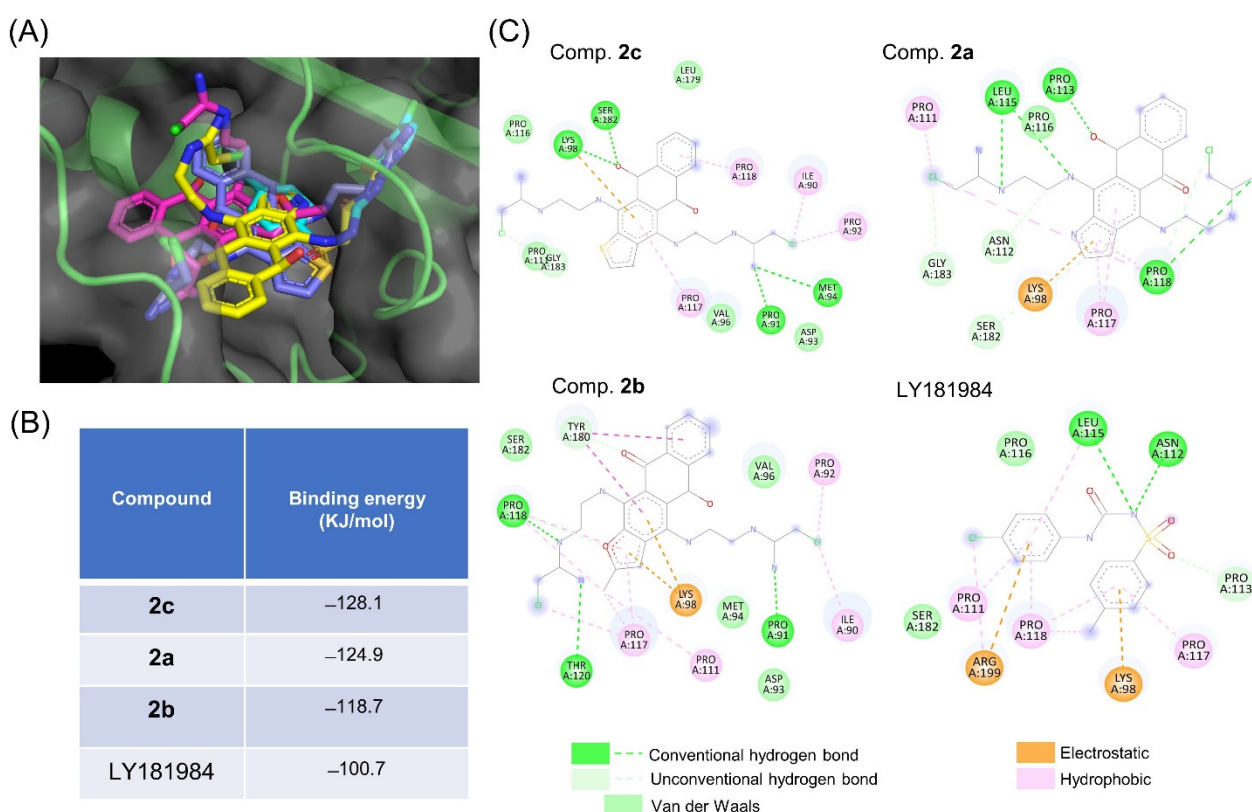

Figure 6. The binding modes of bis(chloroacetamidino)heteroarene-fused anthraquinones **2a–c** and LY181984 after docking into the pocket of tNOX. (**A**) Superimposition of the docked derivative **2c** (purple), derivative **2a** (yellow), derivative **2b** (pink), and LY181984 (cyan). (**B**) The binding energy for individual compound. (**C**) Schematic presentations of the putative tNOX binding modes with the studied derivatives **2a–c** and LY181984. The key residues surrounding the binding pocket of tNOX were identified through the best docking pose of each compound.

4. Discussion

In this report, we describe the design and synthesis of novel antitumor heterocyclic derivatives of anthraquinone, **2a–c**, bearing terminal chloroacetamidines. The modification of the terminal amino groups to chloroacetamidines resulted in high potency against oral cancer cells. Importantly, we further identified tNOX as the protein target of these heteroarene-fused anthraquinones. CETSA, which has recently emerged as a powerful tool for clarifying the binding affinity of drugs to their intracellular protein targets, can be used to identify potent and selective compounds that may serve as potential therapeutic agents in an array of applications [55–57]. Here, we used CETSA and molecular docking simulations to identify and validate tNOX as a key protein target of these novel heteroarene-fused anthraquinones, and we propose that this targeting elicits their anticancer properties.

tNOX has been implicated as a hallmark of cancer cells; it can be suppressed by anticancer drugs to provoke cell death selectively in cancer cells but not in non-transformed cells [25,32,33,58,59]. In this study, we predicted the binding model and docking energy between tNOX and the studied derivatives. Our results indicate that derivatives **2a** and **2c** have lower docking energies (and thus higher predicted affinities) toward tNOX protein, compared to **2b**. The greater binding capacities of derivatives **2a** and **2c** were supported by the results from cell impedance measurements, which were used to assess cell proliferation (Figure 2). Although derivatives **2a**–**c** exhibited similar efficacies against SAS p53-functional cells, we observed differences in their efficacies against p53-mutant HSC-3 cells. In particular, furan-fused anthraquinone **2b** had the least inhibition at 0.5 μM compared to the pyrrole-**2a** and thiophene-**2c** analogs. This suggests that the heterocyclic core critically affects the efficacy of these compounds against p53-mutated cells.

Given that tNOX functions to oxidize the reduced forms of NADH or hydroquinone, its activation increases NAD$^+$ generation, and thereby accelerates proliferation, enhances migration/invasion, and alleviates apoptosis [27–32]. Compounds targeting tNOX protein have been found to suppress cancer cell survival and exhibit therapeutic efficacy [22,33,36,58,60]. However, the underlying mechanisms have not previously been assessed by protein structure predictions and analyses. Based on previous site-directed mutagenesis results [61], we postulated that the NADH-binding motif of tNOX spans from Gly590 to Leu595. The binding sites we predicted herein for the tNOX inhibitor, LY181984, are not near the envisaged NADH binding sites. LY181984 was previously shown to suppress tNOX activity at the plasma membrane of HeLa cells, and to be non-competitive or uncompetitive depending on the concentration of NADH [54]. The consistent interacting residues involved in the van der Waals interactions of the studied derivatives were predicted to be Lys98, Pro117, and Pro118, which also do not reside in the NADH binding sites (Figure 6B,C). We speculate that LY181984 uses a binding mode similar to that of the studied heteroarene-fused anthraquinones, but shows a much lower affinity (−100.7 kJ/mol) (Figure 6B). Given that hydrogen bonding can stabilize the interacted residues, and that derivatives **2a**–**c** were estimated to generate more hydrogen bonds than LY181984, we believe that the enhanced formation of hydrogen bonds may increase the binding affinity between tNOX protein and the studied derivatives [62]. Further experiments, such as efforts to co-crystallize tNOX/inhibitor, are warranted to further explore this possibility.

Another major finding of this study is our clarification that the apoptotic effect of the studied derivatives acts through c-Flip downregulation. c-Flip (cellular FADD-like interleukin 1β-converting enzyme (FLICE) inhibitory protein) acts as an anti-apoptotic protein by interfering with the activation of pro-caspase 8 in the receptor-mediated pathway [63]. Given its anti-apoptotic activity, it is not surprising that c-Flip is upregulated in many cancers and is used as a prognostic marker [64–67]. The transcriptional upregulation of c-Flip is controlled by a set of transcription factors including NFkB, CREB, and EGR1 [68–70]. Meanwhile, c-Flip expression is reportedly attenuated by other transcription factors such as c-Fos, FoxO3a, and c-Myc [71–73]. Cytoplasmically localized Ku70 (a DNA repair factor) is reported to form a complex with c-Flip to enhance its protein stability and thereby shield cells from apoptosis [51]. c-Flip has a rapid turnover rate that is mainly attributed to ubiquitin–proteasomal protein degradation [74]. Post-translational acetylation of Ku70 disrupts its interaction with c-Flip, leaving c-Flip vulnerable to ubiquitination and thereby favoring apoptosis [51,75]. The importance of Ku70 acetylation was highlighted by studies in which deficiency of the deacetylase, SIRT1, was shown to downregulate c-Flip and potentiate TRAIL-induced apoptosis by upregulating c-Myc [50,76,77]. Importantly, we demonstrated herein that the studied novel derivatives may enhance Ku70 acetylation through inhibition of the tNOX–SIRT1 axis, with concurrently increased c-Flip downregulation and provoked apoptosis in oral cancer cells, regardless of p53 functionality.

5. Conclusions

The three heteroarene-fused anthraquinones studied herein target and downregulate tNOX to reduce SIRT1 deacetylase activity and increase Ku70 acetylation, which triggers c-Flip degradation and induces apoptosis in oral cancer cells. Our experimental results and computational evidence suggest that heteroarene-fused anthraquinones may warrant further development as potential cancer therapeutics that act by targeting the tNOX–SIRT1 axis to provoke cancer cell death.

Supplementary Materials: The following supporting information can be downloaded at: https://www.mdpi.com/article/10.3390/cancers14194719/s1, Figure S1: NMR spectra and HPLC chromatograms of bis(chloroacetamidino)heteroareneanthraquinones **2a–c**; Figure S2: The uncropped blots and molecular weight markers in Figure 3; Figure S3: The uncropped blots and molecular weight markers in Figure 4; Figure S4: The uncropped blots and molecular weight markers in Figure 5.

Institutional Review Board Statement: Not applicable.

Informed Consent Statement: Not applicable.

Data Availability Statement: The data presented in this study are available in this article (and supplementary material).

Abbreviations

CETSA	cellular thermal shift assay
c-Flip	cellular FLICE-like inhibitory protein
DIPEA	diisopropylethylamine
ESI	electron spray 118 ionization
HDAC	histone deacetylase
SIRT1	silent mating-type information regulation 1 (Sirtuin 1)
T_M	melting temperature
tNOX	tumor-associated NADH oxidase
Top1	topoisomerase 1

References

1. Faulds, D.; Balfour, J.A.; Chrisp, P.; Langtry, H.D. Mitoxantrone—A Review of Its Pharmacodynamic and Pharmacokinetic Properties, and Therapeutic Potential in the Chemotherapy of Cancer. *Drugs* **1991**, *41*, 400–449. [CrossRef] [PubMed]
2. Stuart-Harris, R.C.; Bozek, T.; Pavlidis, N.A.; Smith, I.E. Mitoxantrone: An active new agent in the treatment of advanced breast cancer. *Cancer Chemother. Pharmacol.* **1984**, *12*, 1–4. [CrossRef] [PubMed]
3. Fox, K.R.; Waring, M.J.; Brown, J.R.; Neidle, S. DNA sequence preferences for the anti-cancer drug mitoxanthrone and related anthraquinones revealed by DNase I footprinting. *FEBS Lett.* **1986**, *202*, 289–294. [CrossRef]
4. Tikhomirov, A.S.; Shtil, A.A.; Shchekotikhin, A.E. Advances in the Discovery of Anthraquinone-Based Anticancer Agents. *Recent Pat. Anti-Cancer Drug Discov.* **2018**, *13*, 159–183. [CrossRef] [PubMed]
5. Tian, W.; Wang, C.M.; Li, D.R.; Hou, H.X. Novel anthraquinone compounds as anticancer agents and their potential mechanism. *Future Med. Chem.* **2020**, *12*, 627–644. [CrossRef]
6. Wright, E.P.; Day, H.A.; Ibrahim, A.M.; Kumar, J.; Boswell, L.J.; Huguin, C.; Stevenson, C.E.; Pors, K.; Waller, Z.A. Mitoxantrone and Analogues Bind and Stabilize i-Motif Forming DNA Sequences. *Sci. Rep.* **2016**, *6*, 39456. [CrossRef]

7. Al-Otaibi, J.S.; Spittle, P.T.; El Gogary, T.M. Interaction of anthraquinone anti-cancer drugs with DNA:Experimental and computational quantum chemical study. *J. Mol. Struct.* **2017**, *1127*, 751–760. [CrossRef]

8. Al-Otaibi, J.S.; El Gogary, T.M. Synthesis of novel anthraquinones: Molecular structure, molecular chemical reactivity descriptors and interactions with DNA as antibiotic and anti-cancer drugs. *J. Mol. Struct.* **2017**, *1130*, 799–809. [CrossRef]

9. Ongaro, A.; Ribaudo, G.; Braud, E.; Etheve-Quelquejeu, M.; De Franco, M.; Garbay, C.; Demange, L.; Gresh, N.; Zagotto, G. Design and synthesis of a peptide derivative of ametantrone targeting the major groove of the d(GGCGCC)(2) palindromic sequence. *New J. Chem.* **2020**, *44*, 3624–3631. [CrossRef]

10. Xie, X.W.; Liu, Z.P.; Li, X. Design, synthesis, bioevaluation of LFC- and PA-tethered anthraquinone analogues of mitoxantrone. *Bioorg. Chem.* **2020**, *101*, 104005. [CrossRef]

11. Chen, C.L.; Liu, F.L.; Lee, C.C.; Chen, T.C.; Chang, W.W.; Guh, J.H.; Ahmed Ali, A.A.; Chang, D.M.; Huang, H.S. Ring fusion strategy for the synthesis of anthra[2,3-d]oxazole-2-thione-5,10-dione homologues as DNA topoisomerase inhibitors and as antitumor agents. *Eur. J. Med. Chem.* **2014**, *87*, 30–38. [CrossRef] [PubMed]

12. Zou, Y.; Cao, Z.; Wang, J.; Chen, X.; Chen, Y.Q.; Li, Y.; Liu, J.; Zhao, Y.; Wang, A.; He, B. A Series of Novel HDAC Inhibitors with Anthraquinone as a Cap Group. *Chem. Pharm. Bull. (Tokyo)* **2020**, *68*, 613–617. [CrossRef] [PubMed]

13. Chen, T.C.; Guh, J.H.; Hsu, H.W.; Chen, C.L.; Lee, C.C.; Wu, C.L.; Lee, Y.R.; Lin, J.J.; Yu, D.S.; Huang, H.S. Synthesis and biological evaluation of anthra [1,9-cd]pyrazol-6(2H)-one scaffold derivatives as potential anticancer agents. *Arab. J. Chem.* **2019**, *12*, 2864–2881. [CrossRef]

14. Wang, Q.; Ma, C.; Li, X.; Wang, X.; Rong, R.; Wei, C.; Zhang, P.; Li, X. Synthesis of novel sugar or azasugar modified anthra[1,2-d] imidazole-6,11-dione derivatives and biological evaluation. *Carbohydr. Res.* **2018**, *460*, 29–33. [CrossRef]

15. Fann, L.Y.; Chen, Y.; Chu, D.C.; Weng, S.J.; Chu, H.C.; Wu, A.T.H.; Lee, J.F.; Ali, A.A.A.; Chen, T.C.; Huang, H.S.; et al. Identification and preclinical evaluation of the small molecule, NSC745887, for treating glioblastomas via suppressing DcR3-associated signaling pathways. *Oncotarget* **2018**, *9*, 11922–11937. [CrossRef] [PubMed]

16. Shchekotikhin, A.E.; Glazunova, V.A.; Dezhenkova, L.G.; Shevtsova, E.K.; Traven, V.F.; Balzarini, J.; Huang, H.S.; Shtil, A.A.; Preobrazhenskaya, M.N. The first series of 4,11-bis[(2-aminoethyl)amino]anthra[2,3-b]furan-5,10-diones: Synthesis and anti-proliferative characteristics. *Eur. J. Med. Chem.* **2011**, *46*, 423–428. [CrossRef]

17. Shchekotikhin, A.E.; Dezhenkova, L.G.; Tsvetkov, V.B.; Luzikov, Y.N.; Volodina, Y.L.; Tatarskiy, V.V., Jr.; Kalinina, A.A.; Treshalin, M.I.; Treshalina, H.M.; Romanenko, V.I.; et al. Discovery of antitumor anthra[2,3-b]furan-3-carboxamides: Optimization of synthesis and evaluation of antitumor properties. *Eur. J. Med. Chem.* **2016**, *112*, 114–129. [CrossRef]

18. Volodina, Y.L.; Dezhenkova, L.G.; Tikhomirov, A.S.; Tatarskiy, V.V.; Kaluzhny, D.N.; Moisenovich, A.M.; Moisenovich, M.M.; Isagulieva, A.K.; Shtil, A.A.; Tsvetkov, V.B.; et al. New anthra[2,3-b]furancarboxamides: A role of positioning of the carboxamide moiety in antitumor properties. *Eur. J. Med. Chem.* **2019**, *165*, 31–45. [CrossRef]

19. Tikhomirov, A.S.; Lin, C.Y.; Volodina, Y.L.; Dezhenkova, L.G.; Tatarskiy, V.V.; Schols, D.; Shtil, A.A.; Kaur, P.; Chueh, P.J.; Shchekotikhin, A.E. New antitumor anthra[2,3-b]furan-3-carboxamides: Synthesis and structure-activity relationship. *Eur. J. Med. Chem.* **2018**, *148*, 128–139. [CrossRef]

20. Tikhomirov, A.S.; Litvinova, V.A.; Andreeva, D.V.; Tsvetkov, V.B.; Dezhenkova, L.G.; Volodina, Y.L.; Kaluzhny, D.N.; Treshalin, I.D.; Schols, D.; Ramonova, A.A.; et al. Amides of pyrrole- and thiophene-fused anthraquinone derivatives: A role of the heterocyclic core in antitumor properties. *Eur. J. Med. Chem.* **2020**, *199*, 112294. [CrossRef]

21. Tikhomirov, A.S.; Shchekotikhin, A.E.; Lee, Y.H.; Chen, Y.A.; Yeh, C.A.; Tatarskiy, V.V., Jr.; Dezhenkova, L.G.; Glazunova, V.A.; Balzarini, J.; Shtil, A.A.; et al. Synthesis and Characterization of 4,11-Diaminoanthra[2,3-b]furan-5,10-diones: Tumor Cell Apoptosis through tNOX-Modulated NAD(+)/NADH Ratio and SIRT1. *J. Med. Chem.* **2015**, *58*, 9522–9534. [CrossRef] [PubMed]

22. Lin, C.Y.; Islam, A.; Su, C.J.; Tikhomirov, A.S.; Shchekotikhin, A.E.; Chuang, S.M.; Chueh, P.J.; Chen, Y.L. Engagement with tNOX (ENOX2) to Inhibit SIRT1 and Activate p53-Dependent and -Independent Apoptotic Pathways by Novel 4,11-Diaminoanthra[2,3-b]furan-5,10-diones in Hepatocellular Carcinoma Cells. *Cancers* **2019**, *11*, 420. [CrossRef] [PubMed]

23. Morre, D.J.; Chueh, P.J.; Morre, D.M. Capsaicin inhibits preferentially the NADH oxidase and growth of transformed cells in culture. *Proc. Natl. Acad. Sci. USA* **1995**, *92*, 1831–1835. [CrossRef]

24. Bruno, M.; Brightman, A.O.; Lawrence, J.; Werderitsh, D.; Morré, D.M.; Morré, D.J. Stimulation of NADH oxidase activity from rat liver plasma membranes by growth factors and hormones is decreased or absent with hepatoma plasma membranes. *Biochem. J.* **1992**, *284 Pt 3*, 625–628. [CrossRef]

25. Chueh, P.J. Cell membrane redox systems and transformation. *Antioxid. Redox Signal.* **2000**, *2*, 177–187. [CrossRef]

26. Chueh, P.J.; Wu, L.Y.; Morre, D.M.; Morre, D.J. tNOX is both necessary and sufficient as a cellular target for the anticancer actions of capsaicin and the green tea catechin (-)-epigallocatechin-3-gallate. *Biofactors* **2004**, *20*, 235–249.

27. Liu, S.C.; Yang, J.J.; Shao, K.N.; Chueh, P.J. RNA interference targeting tNOX attenuates cell migration via a mechanism that involves membrane association of Rac. *Biochem. Biophys. Res. Commun.* **2008**, *365*, 672–677. [CrossRef]

28. Lin, M.H.; Lee, Y.H.; Cheng, H.L.; Chen, H.Y.; Jhuang, F.H.; Chueh, P.J. Capsaicin Inhibits Multiple Bladder Cancer Cell Phenotypes by Inhibiting Tumor-Associated NADH Oxidase (tNOX) and Sirtuin1 (SIRT1). *Molecules* **2016**, *21*, 849. [CrossRef] [PubMed]

29. Cheng, H.L.; Lee, Y.H.; Yuan, T.M.; Chen, S.W.; Chueh, P.J. Update on a tumor-associated NADH oxidase in gastric cancer cell growth. *World J. Gastroenterol.* **2016**, *22*, 2900–2905. [CrossRef]

30. Mao, L.C.; Wang, H.M.; Lin, Y.Y.; Chang, T.K.; Hsin, Y.H.; Chueh, P.J. Stress-induced down-regulation of tumor-associated NADH oxidase during apoptosis in transformed cells. *FEBS Lett.* **2008**, *582*, 3445–3450. [CrossRef]

31. Liu, N.C.; Hsieh, P.F.; Hsieh, M.K.; Zeng, Z.M.; Cheng, H.L.; Liao, J.W.; Chueh, P.J. Capsaicin-mediated tNOX (ENOX2) up-regulation enhances cell proliferation and migration in vitro and in vivo. *J. Agric. Food Chem.* **2012**, *60*, 2758–2765. [CrossRef] [PubMed]

32. Lee, Y.H.; Chen, H.Y.; Su, L.J.; Chueh, P.J. Sirtuin 1 (SIRT1) Deacetylase Activity and NAD(+)/NADH Ratio Are Imperative for Capsaicin-Mediated Programmed Cell Death. *J. Agric. Food Chem.* **2015**, *63*, 7361–7370. [CrossRef] [PubMed]

33. Chen, H.Y.; Islam, A.; Yuan, T.M.; Chen, S.W.; Liu, P.F.; Chueh, P.J. Regulation of tNOX expression through the ROS-p53-POU3F2 axis contributes to cellular responses against oxaliplatin in human colon cancer cells. *J. Exp. Clin. Cancer Res.* **2018**, *37*, 161. [CrossRef] [PubMed]

34. Chen, H.Y.; Cheng, H.L.; Lee, Y.H.; Yuan, T.M.; Chen, S.W.; Lin, Y.Y.; Chueh, P.J. Tumor-associated NADH oxidase (tNOX)-NAD+-sirtuin 1 axis contributes to oxaliplatin-induced apoptosis of gastric cancer cells. *Oncotarget* **2017**, *8*, 15338–15348. [CrossRef] [PubMed]

35. Morre, D.J.; Hostetler, B.; Taggart, D.J.; Morre, D.M.; Musk, A.W.; Robinson, B.W.; Creaney, J. ENOX2-based early detection (ONCOblot) of asbestos-induced malignant mesothelioma 4–10 years in advance of clinical symptoms. *Clin. Proteom.* **2016**, *13*, 2. [CrossRef]

36. Chang, C.F.; Islam, A.; Liu, P.F.; Zhan, J.H.; Chueh, P.J. Capsaicin acts through tNOX (ENOX2) to induce autophagic apoptosis in p53-mutated HSC-3 cells but autophagy in p53-functional SAS oral cancer cells. *Am. J. Cancer Res.* **2020**, *10*, 3230–3247.

37. Ronconi, G.; Lessiani, G.; Spinas, E.; Kritas, S.K.; Caraffa, A.; Saggini, A.; Antinolfi, P.; Pizzicannella, J.; Toniato, E.; Conti, P. ENOX2 (or tNOX): A new and old molecule with cancer activity involved in tumor prevention and therapy. *J. Biol. Regul. Homeost. Agents* **2016**, *30*, 649–653.

38. Davies, S.L.; Bozzo, J. Spotlight on tNOX: A tumor-selective target for cancer therapies. *Drug News Perspect.* **2006**, *19*, 223–225. [CrossRef]

39. Morre, D.J.; Kim, C.; Paulik, M.; Morre, D.M.; Faulk, W.P. Is the drug-responsive NADH oxidase of the cancer cell plasma membrane a molecular target for adriamycin? *J. Bioenerg. Biomembr.* **1997**, *29*, 269–280. [CrossRef]

40. Cogoi, S.; Zorzet, S.; Shchekotikhin, A.E.; Xodo, L.E. Potent Apoptotic Response Induced by Chloroacetamidine Anthrathiophene-diones in Bladder Cancer Cells. *J. Med. Chem.* **2015**, *58*, 5476–5485. [CrossRef]

41. Shchekotikhin, A.E.; Glazunova, V.A.; Luzikov, Y.N.; Buyanov, V.N.; Susova, O.Y.; Shtil, A.A.; Preobrazhenskaya, M.N. Synthesis and structure-activity relationship studies of 4,11-diaminonaphtho[2,3-f]indole-5,10-diones. *Bioorg. Med. Chem.* **2006**, *14*, 5241–5251. [CrossRef] [PubMed]

42. Shchekotikhin, A.E.; Glazunova, V.A.; Dezhenkova, L.G.; Luzikov, Y.N.; Sinkevich, Y.B.; Kovalenko, L.V.; Buyanov, V.N.; Balzarini, J.; Huang, F.C.; Lin, J.J.; et al. Synthesis and cytotoxic properties of 4,11-bis[(aminoethyl)amino]anthra[2,3-b]thiophene-5,10-diones, novel analogues of antitumor anthracene-9,10-diones. *Bioorg. Med. Chem.* **2009**, *17*, 1861–1869. [CrossRef]

43. Chen, C.F.; Huang, S.; Liu, S.C.; Chueh, P.J. Effect of polyclonal antisera to recombinant tNOX protein on the growth of transformed cells. *Biofactors* **2006**, *28*, 119–133. [CrossRef] [PubMed]

44. Smith, T.J. MolView: A program for analyzing and displaying atomic structures on the Macintosh personal computer. *J. Mol. Graph.* **1995**, *13*, 122–125, 115. [CrossRef]

45. Varadi, M.; Anyango, S.; Deshpande, M.; Nair, S.; Natassia, C.; Yordanova, G.; Yuan, D.; Stroe, O.; Wood, G.; Laydon, A.; et al. AlphaFold Protein Structure Database: Massively expanding the structural coverage of protein-sequence space with high-accuracy models. *Nucleic Acids Res.* **2022**, *50*, D439–D444. [CrossRef]

46. Hsu, K.C.; Chen, Y.F.; Lin, S.R.; Yang, J.M. iGEMDOCK: A graphical environment of enhancing GEMDOCK using pharmacological interactions and post-screening analysis. *BMC Bioinform.* **2011**, *12*, 1–11. [CrossRef]

47. Aly, A.A.; Brase, S.; Gomaa, M.A.M. Amidines: Their synthesis, reactivity, and applications in heterocycle synthesis. *Arkivoc* **2018**, *6*, 85–138. [CrossRef]

48. Ichwan, S.J.; Yamada, S.; Sumrejkanchanakij, P.; Ibrahim-Auerkari, E.; Eto, K.; Ikeda, M.A. Defect in serine 46 phosphorylation of p53 contributes to acquisition of p53 resistance in oral squamous cell carcinoma cells. *Oncogene* **2006**, *25*, 1216–1224. [CrossRef]

49. Sakai, E.; Tsuchida, N. Most human squamous cell carcinomas in the oral cavity contain mutated p53 tumor-suppressor genes. *Oncogene* **1992**, *7*, 927–933.

50. Kim, M.J.; Hong, K.S.; Kim, H.B.; Lee, S.H.; Bae, J.H.; Kim, D.W.; Dao, T.T.; Oh, W.K.; Kang, C.D.; Kim, S.H. Ku70 acetylation and modulation of c-Myc/ATF4/CHOP signaling axis by SIRT1 inhibition lead to sensitization of HepG2 cells to TRAIL through induction of DR5 and down-regulation of c-FLIP. *Int. J. Biochem. Cell B* **2013**, *45*, 711–723. [CrossRef]

51. Kerr, E.; Holohan, C.; McLaughlin, K.M.; Majkut, J.; Dolan, S.; Redmond, K.; Riley, J.; McLaughlin, K.; Stasik, I.; Crudden, M.; et al. Identification of an acetylation-dependant Ku70/FLIP complex that regulates FLIP expression and HDAC inhibitor-induced apoptosis. *Cell Death Differ.* **2012**, *19*, 1317–1327. [CrossRef]

52. Martinez Molina, D.; Jafari, R.; Ignatushchenko, M.; Seki, T.; Larsson, E.A.; Dan, C.; Sreekumar, L.; Cao, Y.; Nordlund, P. Monitoring drug target engagement in cells and tissues using the cellular thermal shift assay. *Science* **2013**, *341*, 84–87. [CrossRef]

53. Martinez Molina, D.; Nordlund, P. The Cellular Thermal Shift Assay: A Novel Biophysical Assay for In Situ Drug Target Engagement and Mechanistic Biomarker Studies. *Annu. Rev. Pharmacol. Toxicol.* **2016**, *56*, 141–161. [CrossRef]

54. Morre, D.J.; Wu, L.Y.; Morre, D.M. The antitumor sulfonylurea N-(4-methylphenylsulfonyl)-N′-(4-chlorophenyl) urea (LY181984) inhibits NADH oxidase activity of HeLa plasma membranes. *Biochim. Biophys. Acta* **1995**, *1240*, 11–17. [CrossRef]

55. Yu, J.; Zhang, L.; Peng, J.; Ward, R.; Hao, P.; Wang, J.; Zhang, N.; Yang, Y.; Guo, X.; Xiang, C.; et al. Dictamnine, a novel c-Met inhibitor, suppresses the proliferation of lung cancer cells by downregulating the PI3K/AKT/mTOR and MAPK signaling pathways. *Biochem. Pharmacol.* **2022**, *195*, 114864. [CrossRef]

56. Karvonen, H.; Raivola, J.; Ungureanu, D. Cellular thermal shift assay (CETSA) for determining the drug binding affinity using Ba/F3 clones stably expressing receptor pseudokinases. *Methods Enzymol.* **2022**, *667*, 339–363. [CrossRef]

57. Fang, Z.; Mu, B.; Liu, Y.; Guo, N.; Xiong, L.; Guo, Y.; Xia, A.; Zhang, R.; Zhang, H.; Yao, R.; et al. Discovery of a potent, selective and cell active inhibitor of m(6)A demethylase ALKBH5. *Eur. J. Med. Chem.* **2022**, *238*, 114446. [CrossRef]

58. Sumiyoshi, A.; Shibata, S.; Zhelev, Z.; Miller, T.; Lazarova, D.; Aoki, I.; Obata, T.; Higashi, T.; Bakalova, R. Targeting Glioblastoma via Selective Alteration of Mitochondrial Redox State. *Cancers* **2022**, *14*, 485. [CrossRef]

59. Su, Y.C.; Lin, Y.H.; Zeng, Z.M.; Shao, K.N.; Chueh, P.J. Chemotherapeutic agents enhance cell migration and epithelial-to-mesenchymal transition through transient up-regulation of tNOX (ENOX2) protein. *Biochim. Biophys. Acta* **2012**, *1820*, 1744–1752. [CrossRef]

60. Islam, A.; Hsieh, P.F.; Liu, P.F.; Chou, J.C.; Liao, J.W.; Hsieh, M.K.; Chueh, P.J. Capsaicin exerts therapeutic effects by targeting tNOX-SIRT1 axis and augmenting ROS-dependent autophagy in melanoma cancer cells. *Am. J. Cancer Res.* **2021**, *11*, 4199–4219.

61. Chueh, P.J.; Morré, D.M.; Morré, D.J. A site-directed mutagenesis analysis of tNOX functional domains. *Biochim. Biophys. Acta* **2002**, *1594*, 74–83. [CrossRef]

62. Horowitz, S.; Trievel, R.C. Carbon-oxygen hydrogen bonding in biological structure and function. *J. Biol. Chem.* **2012**, *287*, 41576–41582. [CrossRef]

63. Fulda, S. Tumor resistance to apoptosis. *Int. J. Cancer* **2009**, *124*, 511–515. [CrossRef]

64. Ivanisenko, N.V.; Seyrek, K.; Hillert-Richter, L.K.; Konig, C.; Espe, J.; Bose, K.; Lavrik, I.N. Regulation of extrinsic apoptotic signaling by c-FLIP: Towards targeting cancer networks. *Trends Cancer* **2022**, *8*, 190–209. [CrossRef]

65. Schleich, K.; Buchbinder, J.H.; Pietkiewicz, S.; Kahne, T.; Warnken, U.; Ozturk, S.; Schnolzer, M.; Naumann, M.; Krammer, P.H.; Lavrik, I.N. Molecular architecture of the DED chains at the DISC: Regulation of procaspase-8 activation by short DED proteins c-FLIP and procaspase-8 prodomain. *Cell Death Differ.* **2016**, *23*, 681–694. [CrossRef]

66. Day, T.W.; Huang, S.; Safa, A.R. c-FLIP knockdown induces ligand-independent DR5-, FADD-, caspase-8-, and caspase-9-dependent apoptosis in breast cancer cells. *Biochem. Pharmacol.* **2008**, *76*, 1694–1704. [CrossRef]

67. Riley, J.S.; Hutchinson, R.; McArt, D.G.; Crawford, N.; Holohan, C.; Paul, I.; Van Schaeybroeck, S.; Salto-Tellez, M.; Johnston, P.G.; Fennell, D.A.; et al. Prognostic and therapeutic relevance of FLIP and procaspase-8 overexpression in non-small cell lung cancer. *Cell Death Dis.* **2013**, *4*, e951. [CrossRef]

68. Micheau, O.; Lens, S.; Gaide, O.; Alevizopoulos, K.; Tschopp, J. NF-kappaB signals induce the expression of c-FLIP. *Mol. Cell. Biol.* **2001**, *21*, 5299–5305. [CrossRef]

69. Zhang, J.; Wang, Q.; Zhu, N.; Yu, M.; Shen, B.; Xiang, J.; Lin, A. Cyclic AMP inhibits JNK activation by CREB-mediated induction of c-FLIPL and MKP-1, thereby antagonizing UV-induced apoptosis. *Cell Death Differ.* **2008**, *15*, 1654–1662. [CrossRef]

70. Mahalingam, D.; Natoni, A.; Keane, M.; Samali, A.; Szegezdi, E. Early growth response-1 is a regulator of DR5-induced apoptosis in colon cancer cells. *Br. J. Cancer* **2010**, *102*, 754–764. [CrossRef]

71. Zhang, X.; Zhang, L.; Yang, H.; Huang, X.; Otu, H.; Libermann, T.A.; DeWolf, W.C.; Khosravi-Far, R.; Olumi, A.F. c-Fos as a proapoptotic agent in TRAIL-induced apoptosis in prostate cancer cells. *Cancer Res.* **2007**, *67*, 9425–9434. [CrossRef]

72. Skurk, C.; Maatz, H.; Kim, H.S.; Yang, J.; Abid, M.R.; Aird, W.C.; Walsh, K. The Akt-regulated forkhead transcription factor FOXO3a controls endothelial cell viability through modulation of the caspase-8 inhibitor FLIP. *J. Biol. Chem.* **2004**, *279*, 1513–1525. [CrossRef]

73. Ricci, M.S.; Jin, Z.; Dews, M.; Yu, D.; Thomas-Tikhonenko, A.; Dicker, D.T.; El-Deiry, W.S. Direct repression of FLIP expression by c-myc is a major determinant of TRAIL sensitivity. *Mol. Cell. Biol.* **2004**, *24*, 8541–8555. [CrossRef]

74. Humphreys, L.; Espona-Fiedler, M.; Longley, D.B. FLIP as a therapeutic target in cancer. *FEBS J.* **2018**, *285*, 4104–4123. [CrossRef] [PubMed]

75. Gong, P.; Wang, Y.; Jing, Y. Apoptosis Induction byHistone Deacetylase Inhibitors in Cancer Cells: Role of Ku70. *Int. J. Mol. Sci.* **2019**, *20*, 1601. [CrossRef] [PubMed]

76. Kim, H.B.; Kim, M.J.; Lee, S.H.; Lee, J.W.; Bae, J.H.; Kim, D.W.; Dao, T.T.; Oh, W.K.; Kang, C.D.; Kim, S.H. Amurensin G, a novel SIRT1 inhibitor, sensitizes TRAIL-resistant human leukemic K562 cells to TRAIL-induced apoptosis. *Biochem. Pharmacol.* **2012**, *84*, 402–410. [CrossRef]

77. Kruyt, F.A.E. TRAIL and cancer therapy. *Cancer Lett.* **2008**, *263*, 14–25. [CrossRef]